Letters to the Editors

Xenon Poisoning in a Shut-Down Reactor

The changes in xenon concentration with time, and the ensuing reactivity loss, are well known (*1*) in terms of the flux associated with them. However, in a reactor, account has to be taken of the space dependence of the flux. This may be done by calculating the xenon concentration at various points before proceeding with the reactivity calculations. It is, however, more convenient to determine a flux $\bar{\varphi}$ which is for this purpose representative of the reactor as a whole. This approach has been applied (*2, 3*) to the case of the operating reactor after xenon equilibrium has been reached. It is intended in this note to extend this method to the xenon buildup and decay after the shut-down of a reactor. A more mathematical approach is being published elsewhere (*4*). Here it is intended to combine this with published xenon tables (*5*), thus bringing it into a form suitable for quick use by the reactor operator.

When an effective flux $\bar{\varphi}$ is used, a certain xenon distribution in the core is implied, a distribution which establishes itself as a result of equilibrium at each point between the xenon production (direct from uranium fission and indirect from iodine decay) and the xenon elimination (decay and neutron absorption). The resultant xenon distribution is flatter than the thermal flux distribution because a greater proportion of the available xenon is burnt up in the high flux regions than in the low flux regions of the core. The iodine distribution, on the other hand, is practically identical to the flux distribution, as the iodine neutron absorption is negligible.

The xenon concentration after a large power reduction (to zero power) is composed on the one hand of the xenon due to non-decay of initially-present xenon,[1] and on the other hand of the xenon due to decay of initially-present iodine. When the neutron absorption term in the xenon equilibrium equation is equal to zero, a condition which holds in the present case, the xenon component due to non-decay of available xenon will obviously retain the same distribution in space as that of the saturation xenon. The xenon component due to post-shut-down iodine decay will however have the distribution of the parent iodine, i.e., the same as the thermal flux. Thus, a different effective flux must be used for the xenon which is due to later iodine decay than for xenon which was present as such at the time of the power reduction. In fact the xenon born after the power reduction from iodine decay will be so distributed that relatively more of it will be in the regions of high flux and high importance; the invested reactivity after shut-down is thus greater than that which is estimated by using the same effective flux as during equilibrium power operation.

[1] i.e., that part of the initially-present xenon which has not decayed by the time under consideration.

To determine $\bar{\varphi}$ it is convenient to start from the equation, valid for a point (*1*)

$$X(t) = \frac{\gamma_1 \Sigma_f \varphi_0}{\lambda_2 - \lambda_1}[\exp(-\lambda_1 t) - \exp(-\lambda_2 t)] + \frac{(\gamma_1 + \gamma_2)\Sigma_f \varphi_0}{\lambda_2 + \sigma_2 \varphi_0} \exp(-\lambda_2 t) \quad (1)$$

where $X(t)$ is the xenon concentration after shut-down, λ_1 and λ_2 are the decay constants of iodine and of xenon, γ_1 and γ_2 are the direct fission yields of iodine and xenon, Σ_f is the macroscopic fission cross section of the fuel, σ_2 is the microscopic absorption cross section of xenon-135, and φ_0 is the thermal flux during operation. The reactivity ρ associated with a given xenon concentration at a uniform flux is (*1*)

$$\rho = -\frac{X(t)\sigma_2 f}{\Sigma_u} \quad (2)$$

where Σ_u is the macroscopic absorption cross section of the fuel and f is the thermal utilization factor of the unpoisoned core. Thus,

$$-\rho = A[\exp(-\lambda_1 t) - \exp(-\lambda_2 t)]\varphi_0 + B\frac{\exp(-\lambda_2 t)\varphi_0}{1 + \sigma_2/\lambda_2)\varphi_0} \quad (3)$$

where A and B are constants.

The first term in the above equation is due to xenon born from iodine after the power reduction had taken place, while the second term is due to xenon present as such at the time of the power reduction.

In order to overcome the restricting assumption of uniform flux, we now define average effective fluxes $\bar{\varphi}_1$ and $\bar{\varphi}_2$ in such a manner that

$$-\rho = A[\exp(-\lambda_1 t) - \exp(-\lambda_2 t)]\bar{\varphi}_1 + B\frac{\exp(-\lambda_2 t)\bar{\varphi}_2}{1 + (\sigma_2/\lambda_2)\bar{\varphi}_2} \quad (4)$$

holds for the core as a whole. For this purpose, suitable values $\bar{\varphi}_1$ and $\bar{\varphi}_2$ must be determined.

The total reactivity loss is the local loss weighted by the product of the flux φ and the importance φ^* relevant at the time considered, and integrated over the reactor. Thus, from Eq. (3),

$$-\rho = \frac{\int A[\exp(-\lambda_1 t) - \exp(-\lambda_2 t)]\varphi_0 \varphi\varphi^* \, dv}{\int \varphi\varphi^* \, dv} + \frac{\int B\frac{\exp(-\lambda_2 t)}{1 + (\sigma_2/\lambda_2)\varphi_0}\varphi_0 \varphi\varphi^* \, dv}{\int \varphi\varphi^* \, dv} \quad (5)$$

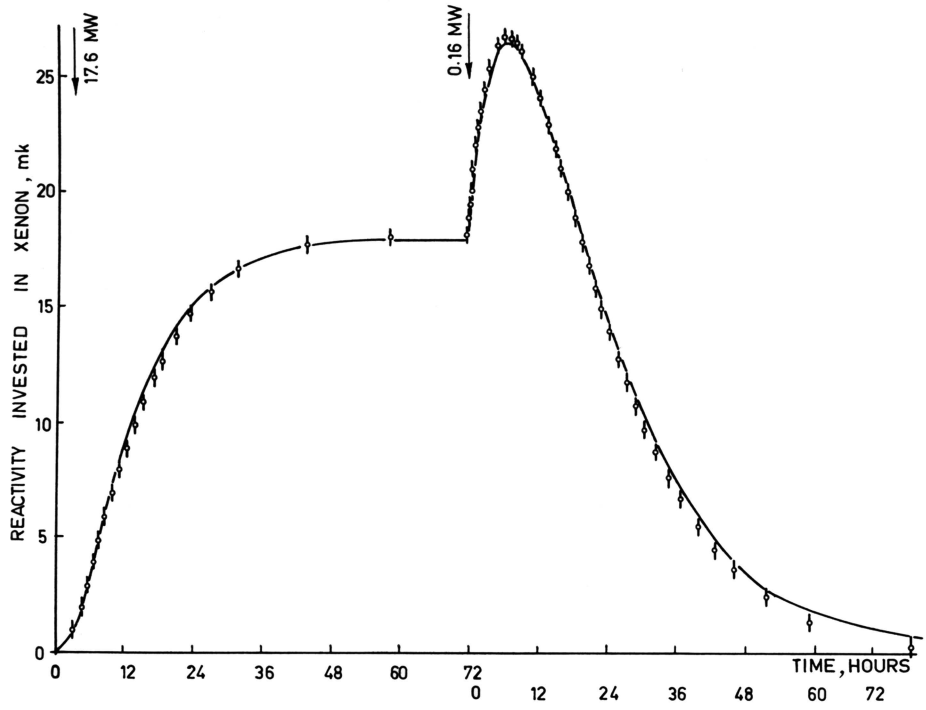

FIG. 1. Xenon build-up and decay in the Diorit reactor. Points are experimental results. Line was calculated using the theory developed in this note.

These simplified equations hold only if the fast and thermal adjoint fluxes have the same shape. Since the integration covers the core only and excludes the reflector this approximation does not introduce an appreciable error when applied to the Swiss heavy water reactor Diorit.

Comparing Eq. (4) and Eq. (5) one gets

$$\bar{\varphi}_1 = \left(\int \varphi_0 \varphi\varphi^* \, dv \Big/ \int \varphi\varphi^* \, dv \right) \tag{6a}$$

and

$$\bar{\varphi}_2 = \left(\int \frac{\varphi_0 \varphi\varphi^*}{1 + (\sigma_2/\lambda_2)\varphi_0} \, dv \Big/ \int \frac{\varphi\varphi^*}{1 + (\sigma_2/\lambda_2)\varphi_0} \, dv \right) \tag{6b}$$

It is seen from the above that, in general, the use of two average fluxes enables the calculations of xenon poisoning after shut-down to be carried through. These effective flux values are independent of time; that is, although the xenon distribution in the reactor changes after shut-down, it can be broken down into two separate components which retain their respective original distributions. It is the change in the relative contribution of each of these components as a function of time which causes the change in the over-all form.

At the time of the power reduction, the contribution of the $\bar{\varphi}_1$ component is by definition zero. The average effective flux is then $\bar{\varphi}_2$, which is thus also the average flux for poisoning after equilibrium has been reached at power operation.

The distinction between the two components of the shut-down xenon poisoning makes the use of published xenon tables (*5*) possible. These tables are in fact a tabulation of the time functions of xenon buildup and decay, and must be used with suitable initial iodine and xenon concentrations. The tables have to be entered at the appropriate power density level, and it is here that the average flux values are relevant. It is evident from the above that for the case of the reactor after shut-down, the initial iodine value to be used is that obtained during steady state operation at a flux $\bar{\varphi}_1$, and the initial xenon value is that associated with a flux $\bar{\varphi}_2$.

For the Swiss heavy water reactor Diorit, the values of $\bar{\varphi}_1$ and $\bar{\varphi}_2$ have been calculated as 0.61 and 0.67 $\hat{\varphi}$ respectively, where $\hat{\varphi}$ is the flux at the center of the core. Although both xenon and iodine ("latent" xenon) were built up at the same time, the xenon born from iodine after shut-down is seen to be associated with a higher average flux than the xenon present as such during operation.

A special xenon run was made in the Diorit reactor. The xenon was first allowed to build up at a power of 17.6 mw ($\hat{\varphi} = 2.2 \times 10^{13}$ neutrons/cm^2 sec) and the power then reduced to 160 kw. The reactivity invested in xenon was measured on calibrated fine control rods. Figure 1 shows the xenon build up and decay measured in this experiment, as well as the theoretical curve calculated from the tables (*5*) using $\bar{\varphi}_2$ for the power operation period and $\bar{\varphi}_1$ and $\bar{\varphi}_2$ for the-down period. Calculations using $\bar{\varphi}_2$ only, even after the power reduction, resulted in the magnitude of the xenon peak being underestimated by some 2.5 mk.

It can be seen that using a relatively simple procedure, based on elementary perturbation theory, good agreement is found between experimentally determined xenon poisoning values and theoretical predictions. The experimentally determined xenon poisoning value is based on comparison with a carefully calibrated fine control rod, which was repeatedly shifted in order to cover the whole reactivity range of the xenon effect. The fact that a careful experiment and the above described theoretical procedure resulted in consistent values for the xenon poisoning gave us confidence

to use this poisoning effect for the calibration of our coarse control rod bank. In fact we consider the reactivity value of the coarse control rod bank obtained from the comparison with xenon poisoning the most reliable value (*6*).

REFERENCES

1. S. GLASSTONE AND M. C. EDLUND, "The Elements of Nuclear Reactor Theory." Van Nostrand, Princeton, New Jersey, 1952.
2. R. L. MURRAY, "Nuclear Reactor Physics." Prentice Hall, Englewood Cliffs, New Jersey, 1957.
3. A. M. WEINBERG AND E. P. WIGNER, "The Physical Theory of Neutron Chain Reactors." Univ. of Chicago Press, Chicago, Illinois, 1958.
4. W. HÄLG, S. RAVANI, H. ALBERS, AND Z. J. DORON, *Z. angew. Math. u. Physik* **14,** (1963).
5. H. K. CLARK AND J. C. ENGLISH, Xenon tables. DP-200 (May 1957).
6. H. ALBERS, Z. J. DORON, AND T. GOZANI, *Neue Technik*, **4,** 461 (1962).

H. ALBERS
AND Z. J. DORON*

Swiss Federal Institute for Reactor Research
Würenlingen, Switzerland

W. HÄLG
AND S. RAVANI

Swiss Federal Institute of Technology
Zurich, Switzerland

Received July 10, 1962
Revised November 19, 1962

* Z. J. Doron is on leave from the Israel Atomic Energy Commission.

Nonperturbing Foils—An Experimental Verification*

Neutron detecting foils which have the capability of measuring thermal neutron flux without introducing flux perturbation have been proposed in an earlier publication (*1*) which presented the theory of the nonperturbing foils and gave preliminary experimental verification. The method is intended for use in regions where the thermal flux is due to a uniform slowing down source. A double P_0 calculation indicates that the nonperturbing condition exists when the moderating ratio of the foil equals that of the medium in which the measurement is performed. This matching condition establishes foil parameters such that the ratio of the production rate of thermal neutrons which slow down in the foil to the absorption rate of the foil is equal to that of the medium. It is felt that there is sufficient promise in this technique to warrant an accurate verification that these foils cause no perturbation. It is the purpose of this article to present experimental data substantiating the nonperturbing nature of these foils.

To accomplish this verification, two methods are used. The first, and most direct, is to show that foils whose thicknesses vary by a factor of four yield the same specific activity. The other method is to show that the specific activity of these foils is equal to the unperturbed value as determined by an extrapolation method for metal foils.

The medium selected for this experimental investigation was water. The test section consisted of a triangular array of 1-curie neutron sources with the test section in the geometric center. This assembly is described in detail in ref. *2*. The test section provided a thermal flux which was spatially invariant over ±5.3 mean free paths in water in the horizontal plane and ±2.7 mean free paths in the vertical plane. Thus, the unperturbed flux through the region occupied by the foils remained constant in spite of the wide variation in foil thickness.

For ease of fabrication, the matching foils were prepared in liquid form. The foil material used consisted of a solution of 99.8% D_2O and 0.2% H_2O, and which contained 2.90 gm/liter of metallic indium in the form of indium nitrate. This solution has a moderating ratio equal to that of water. The high D_2O concentration was used to allow the maximum concentration of indium since the flux in the test section was low. The cylindrical liquid foil containers were fabricated from $\frac{1}{16}$ in. thick lucite with an internal diameter of 2 cm and thicknesses from $\frac{1}{16}$ in. to $\frac{1}{4}$ in. The metal foils were also fabricated 2 cm in diameter with thicknesses that ranged from 0.0006 in. to 0.005 in. All of the foils were supported on mylar or polyethylene tape attached to $1\frac{3}{4}$ in. lucite rings. Cadmium covers, 0.040 in. thick, were fabricated for all foils.

The metal foils were activated in the test section and counted at the center of two 2 in. x 2 in. NaI(Tl) crystals spaced 2 cm apart. It was experimentally verified that this assembly eliminated geometry and self-absorption variations due to changes in foil thickness. This assembly was also used to determine the "unperturbed" activity as measured by a $\frac{1}{16}$ in. thick matching foil. It was not convenient to use this counting system for the thicker matching foils since their greater size introduced significant geometry corrections. To reduce the variation in counting efficiencies, these foils were integrally counted in the 1 in. diam well of a $1\frac{3}{4}$ in. diam by 2 in. long NaI(Tl) scintillation crystal. Variation in counting efficiencies and self-absorption between the various foil thicknesses were corrected experimentally by activating some foil material in the AGN-201 reactor and filling the various size foil containers with this material. Each container was then counted in the well crystal and the correction factors obtained. The maximum correction was only 4.2%.

The specific activities of the bare and cadmium covered matching foils are shown in Fig. 1 for thicknesses of $\frac{1}{16}$ in. to $\frac{1}{4}$ in. Each point represents an average of five separate runs. The standard deviation of each point due to counting statistics in less than 0.5%. Straight lines were fitted to these data by the method of least squares. The curve representing activity due to the thermal neutron flux was determined by subtracting the two curves. To allow a close inspection of these results, it is necessary to examine the equations obtained from the analysis. These are

$$\text{Bare} \qquad \frac{A_\infty}{m} = 329.04 - 0.11x \tag{1}$$

$$\text{Cd} \qquad \frac{A_\infty}{m} = 77.07 + 0.77x \tag{2}$$

$$\text{Thermal} \qquad \frac{A_\infty}{m} = 251.97 - 0.88x \tag{3}$$

* This work was supported in part under a research grant from the Texas Engineering Experiment Station.